Available online at www.sciencedirect.com
ScienceDirect
Journal of Sound and Vibration 299 (2007) 261–282
JOURNAL OF SOUND AND VIBRATION
www.elsevier.com/locate/jsvi

Model-based control of combustion instabilities

A.S. Morgans*, A.P. Dowling

Department of Engineering, University of Cambridge, Cambridge, CB2 1PZ, UK

Received 27 January 2006; received in revised form 5 July 2006; accepted 26 July 2006
Available online 27 September 2006

Abstract

Model-based active controllers are designed for two laboratory combustion systems exhibiting a combustion instability, a simple Rijke tube and an atmospheric pressure combustion rig. The unstable open-loop transfer functions (OLTFs) of both are measured experimentally using an actuator signal which is comprised of two components; a control signal from an empirically obtained controller, and a wide-bandwidth signal for identification of the transfer function. This method of measuring the OLTF could be applied equally well at full scale. Robust model-based controllers are designed for both systems using linear Nyquist techniques, and are implemented experimentally. Both sets of controllers stabilise their system (even from within the limit cycle resulting from instability), with a reduction of 80 dB at the Rijke tube microphone and a reduction of approximately 40 dB at the combustion rig pressure transducer. In addition, both sets of controllers are demonstrated to control the system beyond the operating conditions which they were designed for, demonstrating the advantages of robust model-based controllers.

1. Introduction

Combustion instabilities are caused by a coupling between acoustic waves and unsteady heat release. Unsteady combustion is an efficient acoustic source [1,2], combustors tend to be highly resonant systems and acoustic waves cause variations in unsteady heat release [3]. Therefore, when unsteady heat release generates acoustic waves, these reflect from the boundaries of the combustor to produce flow unsteadiness near the flame, further perturbing the heat release. Depending on the phase relationship, acoustic waves may successively increase in energy, leading to large amplitude self-excited oscillations. These are often energetic enough to cause severe structural damage to the system.

Combustion instabilities occur in a wide range of combustion systems, including gas turbine combustors in aero-engines [4], industrial land-based gas turbines [5,6], ramjets and aero-engine afterburners. They are of particular current concern as the next generation of low NO_x gas turbine combustors are especially susceptible to them.

To eliminate combustion instabilities, the coupling between the acoustic waves and the unsteady heat release must be interrupted. This can be achieved using passive control methods [7,8], which may either seek to reduce the susceptibility of the combustion process to acoustic excitation, or to remove energy from the sound

*Corresponding author.
E-mail address: asm28@cam.ac.uk (A.S. Morgans).

0022-460X/$ - see front matter © 2006 Elsevier Ltd. All rights reserved.
doi:10.1016/j.jsv.2006.07.014

waves. Ad hoc hardware design changes such as modifying the fuel injection system or combustor geometry [9,3] are based on the former approach, while acoustic dampers such as Helmholtz resonators, quarter wave tubes, perforated plates or acoustic liners [10,11] are based on the latter. The problem with passive approaches is that they tend to be effective only over a limited range of operating conditions, they may be ineffective at the low frequencies at which some of the most damaging instabilities occur and the changes of design involved are usually costly and time-consuming.

Active feedback control provides another means of interrupting the coupling between acoustic waves and unsteady heat release [12,13]. An actuator modifies some system parameter in response to a measured sensor signal. The aim is to design the controller (the relationship between the sensor signal and the signal used to drive the actuator) such that the unsteady heat release and acoustic waves interact differently, leading to decaying rather than growing oscillations. Typical sensor signals include pressure measurements from microphones or pressure transducers [14–16] and, if there is optical access to the system, chemiluminescence measurements from a photomultiplier [17]. Practical actuation is most commonly achieved by unsteady modulation of the fuel supply. This has been demonstrated experimentally [18–20,17] and at full-scale [14,5], although obtaining a suitable valve for fuel modulation remains a challenge. Controller design for combustion systems is made particularly challenging by factors such as large time delays, high background noise levels and the potential for multiple instability modes [6,21]. In the past, approaches to controller design were somewhat empirical, but more systematic approaches such as robust model-based control and adaptive control are now being promoted [12].

Model-based controllers require some knowledge of the open-loop system to be controlled, which may be obtained through either modelling or measurement. The vast majority of model-based controllers designed for combustion instabilities so far have been based on mathematical rather than measured models [22–24]. This is because during instability, the required linear open-loop transfer function (OLTF) is masked by a nonlinear limit cycle in which the oscillation amplitude is limited by saturation effects in the heat release rate [25], making direct measurement of it difficult. Furthermore, the consequences of instability may be so severe that measurement of the system is impractical. However, because combustion systems involve complicated processes, such as turbulence and combustion itself, which are hard to model accurately, controller designs based on mathematical models are unlikely to be sufficiently accurate for use in full-scale combustion systems. It is therefore preferable for controller design to be based on measurement of the system. Two examples in which model-based controller design was based on system measurement are a Rijke tube in which the system at the unstable operating point was deduced by measurement of a nearby stable operating point and extrapolation [26], and a spray combustor in which the nonlinear limit cycle was used as an approximation to the linear OLTF [27].

The aim of the work in this paper is to design robust model-based controllers for two unstable combustion systems, based on system measurements. The first system is a Rijke tube, which provides the simplest laboratory-scale demonstration of combustion instabilities [28]. The second is an atmospheric combustor rig, designed to model the fuel injection/premix ducts found on each of the nine combustion chambers on the Rolls-Royce RB211-DLE industrial gas turbine. To overcome the difficulties associated with measurement of unstable systems, a method of using an empirically obtained controller (which may have poor robustness properties) to stabilise the system, and superimposing a high bandwidth signal for system identification was used. Such an approach could be extended to larger scale combustion systems: simple empirically chosen controllers are easily found for many combustion systems [5,29–31]. These then allow accurate measurement of the unstable OLTF so that controllers with improved performance and robustness can be designed.

2. The Rijke tube

The Rijke tube provides the simplest means of obtaining combustion instabilities on a laboratory scale. Although it well-known that Rijke tubes can be stabilised using active control [32–34], a Rijke tube is considered here to illustrate some principles concerning transfer function measurement and the advantages of robust controller design. These principles remain relevant when applied to more complex systems exhibiting combustion instabilities.

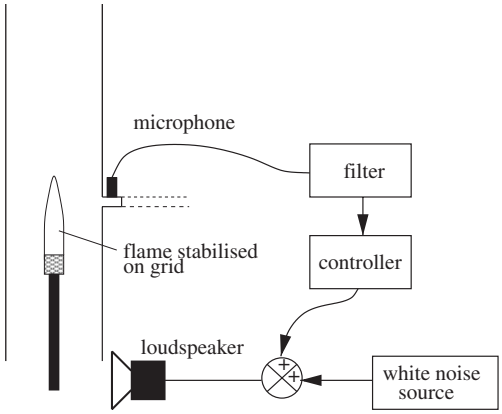

Fig. 1. Experimental set-up of the Rijke tube.

The Rijke tube used was a vertical quartz tube of length 0.75 m and diameter 44 mm, as shown in Fig. 1. A propane-fuelled Bunsen burner provided a laminar flame, which was stabilised on a grid 0.225 m above the bottom of the tube. In the absence of control, the Rijke tube exhibited an instability at 1533 rads^{-1} (244 Hz). A microphone was fitted to a tube tapping 0.34 m from the bottom of the tube, using the semi-infinite line technique to obtain thermal insulation without distortion from acoustic reflections. Actuation was achieved using a 50 W low-frequency loudspeaker situated close to the lower end of the tube. The loudspeaker was chosen to have a flat response over the frequency range of interest (500–12 600 rads^{-1} or 80–2000 Hz); above and below this frequency range, its dynamics became more complicated. Control algorithms were implemented on a 32-bit digital signal processing (DSP) board, and unsteady measurements were recorded using a PC-based data-acquisition system.

2.1. Measuring the OLTF

The OLTF needed for control purposes is from the actuator signal to the sensor signal, in this case from the loudspeaker voltage to the microphone reading. As with all naturally unstable systems, measurement of this OLTF is complicated by the fact that during instability, nonlinear limit cycle behaviour dominates and masks the linear relationship that would be observed at low oscillation amplitudes. In order to prevent the growth of small perturbations, the measurement of linear behaviour is required for controller design.

To overcome this problem, a loudspeaker voltage was used which was comprised of two components:

1. A control signal from a trial-and-error controller to eliminate the nonlinear limit cycle.[1]
2. A wide bandwidth signal, in this case, white noise signal from a white noise generator, for identification of the OLTF.

The voltage was applied to the loudspeaker, the response of the microphone recorded and the ratio of the Fourier transforms used to deduce the OLTF. It was important to use the total loudspeaker voltage in deducing the OLTF, not just the white noise component. Care was taken to ensure that each Fourier transform sample set contained the full range of frequencies. Although the controller signal caused the loudspeaker input spectrum to have a peak at the unstable frequency, applying loud enough white noise ensured that this peak did not rise significantly above the white noise level. Because the loudspeaker dynamics are likely to become complicated at very low and high frequencies, a bandpass filter with a passband from 500 to 12 600 rads^{-1} (80–2000 Hz) was applied to the sensor signal.

[1]The trial-and-error controller was a phase-lead compensator, whose arguments had been estimated using measurement of the transfer function during the limit cycle and reversing the phase change across the unstable mode. These coefficients were then varied using trial-and-error, until a stabilising controller was obtained.

2.2. Analytical model

To provide an insight into the unstable behaviour of the Rijke tube, a mathematical model, based on previous work [35,36,13], was considered. The frequencies were assumed sufficiently low for the combustion zone to be compact and for only one-dimensional disturbances to be important. Entropy waves and the mean flow were neglected, and the speed of sound and mean density throughout the tube were assumed constant (it has been shown that these modest changes in $\overline{\rho}$ and $\overline{c}$ have little influence on the stability behaviour of the system [33]). The model parameters are shown in Fig. 2. Distance along the tube is denoted by x with the heat source at $x = 0$ and the bottom and top of the tube at $x = -x_b$ and $x = x_t$, respectively. These boundaries have pressure reflection coefficients R_b and R_t, respectively; both will have values close to -1 due to the atmospheric pressure condition at the open tube ends. The loudspeaker emits a pressure signal $L(t)$.

Below and above the combustion zone (separately), the pressure obeys the linear wave equation. Denoting below and above the combustion zone by the subscripts 1 and 2, respectively, the pressure and velocity can be written as

$$p(x,t) = A_i\left(t - \frac{x}{\overline{c}}\right) + B_i\left(t + \frac{x}{\overline{c}}\right), \quad u(x,t) = \frac{A_i}{\overline{\rho}\,\overline{c}}\left(t - \frac{x}{\overline{c}}\right) - \frac{B_i}{\overline{\rho}\,\overline{c}}\left(t + \frac{x}{\overline{c}}\right). \tag{1}$$

The reflection coefficients at the tube ends allow the inward travelling wave amplitudes, A_1 and B_2, to be expressed in terms of the outward travelling wave amplitudes, B_1 and A_2, respectively. Note that below the combustion zone, the inward travelling wave also includes a component from the loudspeaker signal, which at the combustion zone is equal to $L(t - x_b/c)$. To relate the acoustic wave amplitudes either side of the combustion zone, the linearised flow conservation equations [37] are applied across it. These require zero pressure difference and a velocity change that is related to the heat release rate per unit cross-sectional area. Applying these equations, taking Laplace transforms and substituting in the flame transfer function, $q(s) = \overline{\rho}\,\overline{c}^2 H(s)u_1(s)$ (where q is the instantaneous rate of heat release per unit area and u_1 is the fluid velocity just below the combustion zone), the outward travelling wave amplitudes can be related to the loudspeaker pressure signal through the following matrix equation:

$$\begin{bmatrix} -1 - R_b e^{-s\tau_b} & 1 + R_t e^{-s\tau_t} \\ \dfrac{(1+(\gamma-1)H(s))(1-R_b e^{-s\tau_b})}{\gamma-1} & \dfrac{1-R_t e^{-s\tau_t}}{\gamma-1} \end{bmatrix} \begin{bmatrix} B_1(s) \\ A_2(s) \end{bmatrix} = \begin{bmatrix} e^{-sx_b/\overline{c}} \\ \dfrac{(1+(\gamma-1)H(s))}{\gamma-1} e^{-sx_b/\overline{c}} \end{bmatrix} L(s). \tag{2}$$

For a pressure sensor above the combustion zone, it is necessary to obtain the transfer function from the loudspeaker signal, $L(t)$, to the upward travelling pressure wave above the combustion zone, $A_2(t)$. Both sides of Eq. (2) can be premultiplied by the inverse of the matrix on the left-hand side. If the determinant of

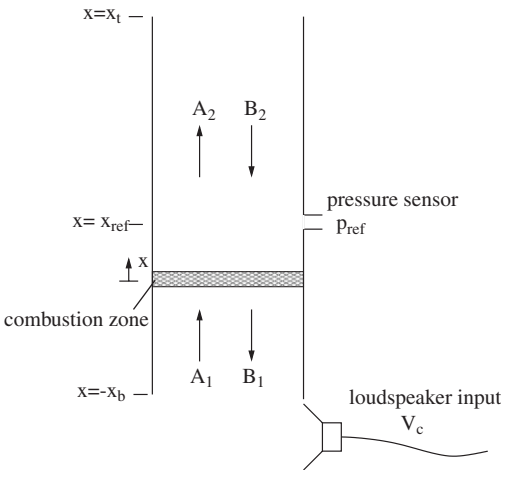

Fig. 2. Diagram of the Rijke tube model.

this matrix is J then

$$\frac{A_2(s)}{L(s)} = \frac{-2e^{-sx_b/\overline{c}}}{(\gamma-1)J}(1+(\gamma-1)H(s)). \tag{3}$$

The OLTF required, $G_m(s)$, is from the loudspeaker input, V_c, to the microphone pressure, p_{ref}. This can be obtained from Eq. (3) by relating the loudspeaker input and output by $W_{\text{ac}}(s) = L(s)/V_c(s)$, where $W_{\text{ac}}(s)$ is the loudspeaker transfer function, and by expressing p_{ref} in terms of the acoustic waves above the combustion zone. Over the frequencies of interest, the loudspeaker dynamics are known to be flat and so $W_{\text{ac}}(s)\sim$ constant.

$$\frac{p_{\text{ref}}(s)}{V_c(s)} = \frac{-2W_{\text{ac}}(s)e^{-s(x_{\text{ref}}+x_b)/\overline{c}}}{(\gamma-1)J}(1+R_t e^{-2s(x_t-x_{\text{ref}})/\overline{c}})(1+(\gamma-1)H(s)). \tag{4}$$

To evaluate this OLTF, a form must be assumed for the flame transfer function, $H(s)$. The simplest type of flame model, based on a time-lag concept, is assumed in which $H(s) \propto e^{-s\tau_H}$. Substituting in for the geometry and flow parameters, the predicted OLTF was evaluated. For comparison with the experiments, values of $x_b = 0.25\,\text{m}$, $x_t = 0.5\,\text{m}$, $x_{\text{ref}} = 0.09\,\text{m}$, $R_b = R_u = -0.90$, $W_{\text{ac}} = -5$ (the negative sign is needed to match the low-frequency phase response) and $\gamma = 1.4$ were used. The flame model time delay was chosen to be $\tau_H = 0.9\,\text{ms}$ and the speed of sound $\overline{c} = 375\,\text{m s}^{-1}$. A measurement time delay of 0.6 ms was added to the phase response. The OLTF was considered both in the absence ($H(s) = 0$, $\overline{c} = 340\,\text{m s}^{-1}$) and presence (above values) of a flame.

2.3. The OLTF

The experimentally measured OLTF is shown in Fig. 3 and the OLTF, as predicted by the mathematical model, is shown in Fig. 4. To reveal the influence of combustion, both are plotted in the presence and absence of a flame.

For the transfer functions in the absence of a flame, both the magnitude and phase responses are in excellent agreement. In the presence of the flame, the agreement is still good, although the pole-zero cancellations (for example between the pairs of zeros/poles either side of 3000, 6000, 8000 rads^{-1}) are far more pronounced for the measured OLTF. The magnitude peaks represent system resonances and correspond to the various "organ-pipe" modes of the acoustic waves in an open-ended tube. The shift to higher frequencies in the presence of combustion is due to the increase in mean temperature.

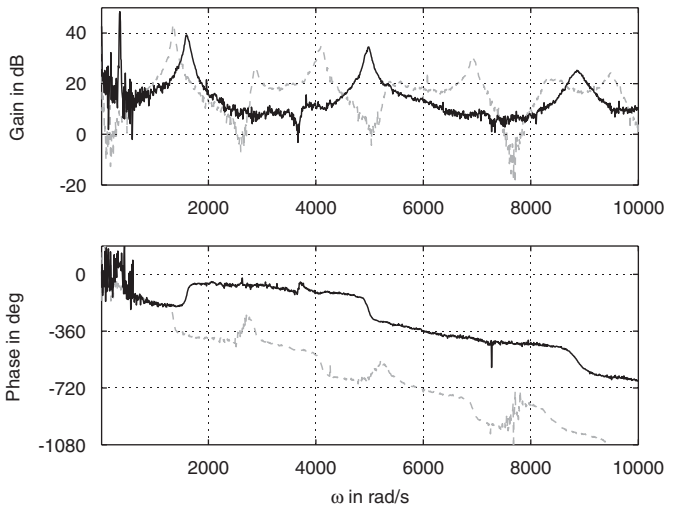

Fig. 3. The measured open-loop transfer function of the Rijke tube: —, with flame; - - -, without flame.

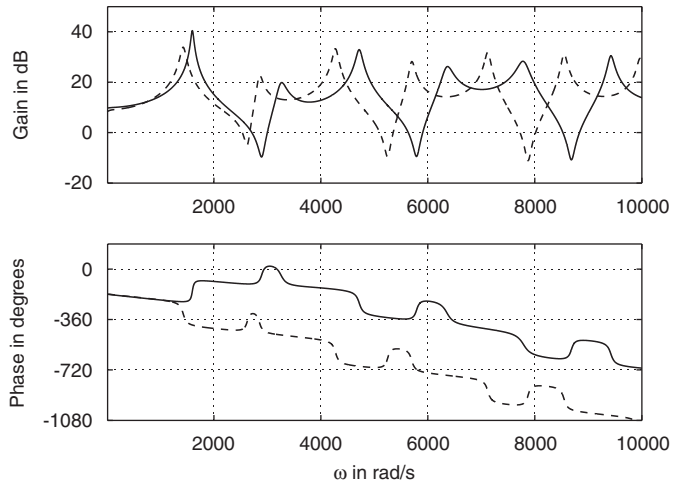

Fig. 4. The predicted open-loop transfer function of the Rijke tube: —, with flame: - - -, without flame.

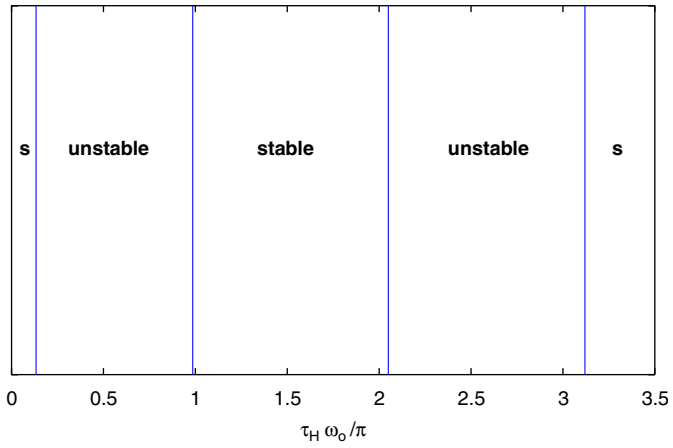

Fig. 5. The stability regions of the first mode of the Rijke tube as a function of the heat release time delay, τ_H.

By considering each modal peak to be caused by a second-order transfer function, stability information can be deduced from the phase change across the modal peaks. A phase increase of 180° indicates an unstable conjugate pair of poles while a phase decrease of 180° indicates a stable conjugate pair. In the absence of combustion, all modes are stable. This is unsurprising, given the absence of any coupling mechanism to cause instability. With combustion, the measured transfer function shows that the first (fundamental) mode has become unstable, with all other modes remaining stable. The same is true in the predicted transfer function, although stability is found to depend strongly on the value of the flame model time delay, τ_H. As shown in Fig. 5, successive changes in τ_H of approximately π/ω_o cause the stability of the first mode to alternate (where ω_o is the theoretical first mode frequency corresponding to a wavelength of double the tube length). This corresponds to the intervals at which the heat release changes phase by 180°, and therefore would be expected from Rayleigh's criterion. The agreement between the measured and predicted transfer functions provides physical insight into the measured transfer function, showing that the instability arises due to the relationship between heat release and acoustic waves, and may be caused entirely by linear effects.

2.4. Controller design

To eliminate the complicated loudspeaker dynamics, the bandpass filter was applied to the microphone signal. The measured OLTF from the loudspeaker input to the filtered microphone voltage, $G(s)$, was then used in controller design. The Bode and Nyquist plots for this OLTF are shown in Figs. 6 and 7. The main effect of the filter on the pass-band is to introduce a time delay of about 0.5 ms, which manifests itself as an additional phase gradient. The magnitude shift in the Bode diagram relative to Fig. 3 is due to microphone voltage rather than microphone pressure now being used.

The system is single-input single-output and so Nyquist techniques provide a suitable means of designing robust controllers. With this technique, the measured OLTF can be used directly in controller design: subject to the system having low noise, there is no need to model or approximate what has been measured. According to the Nyquist criterion, a negative feedback system such as that in Fig. 8 is stable if the number of

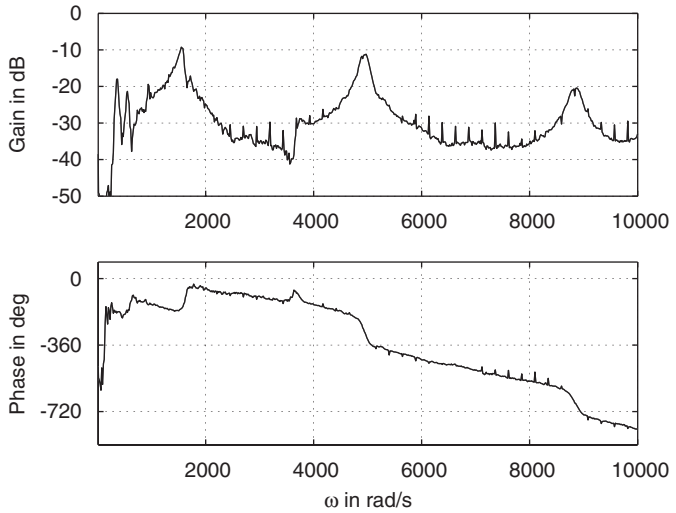

Fig. 6. Bode diagram for the OLTF from the loudspeaker voltage to the filtered microphone voltage.

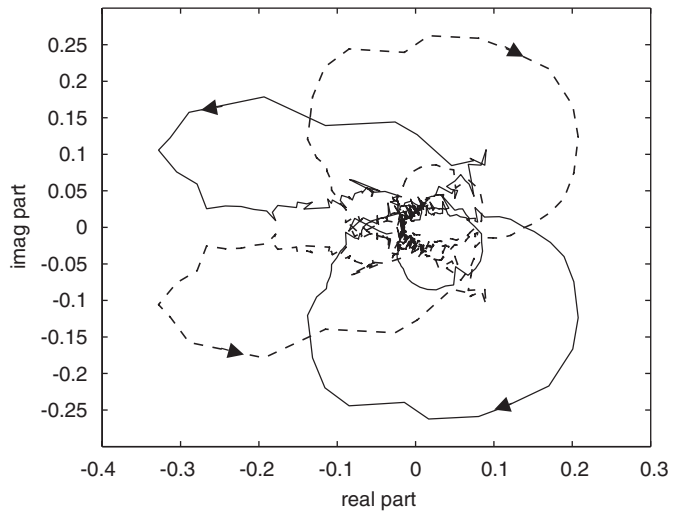

Fig. 7. Nyquist diagram for the OLTF from the loudspeaker voltage to the filtered microphone voltage: —, $G(\mathrm{i}\omega)$ for positive ω; - - -, $G(\mathrm{i}\omega)$ for negative ω.

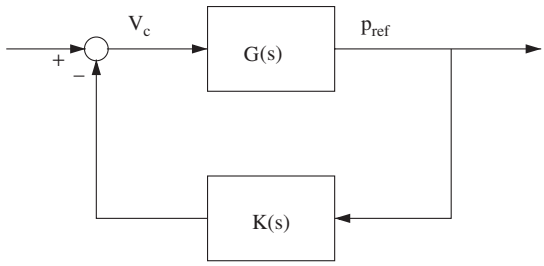

Fig. 8. The structure of a negative feedback control system.

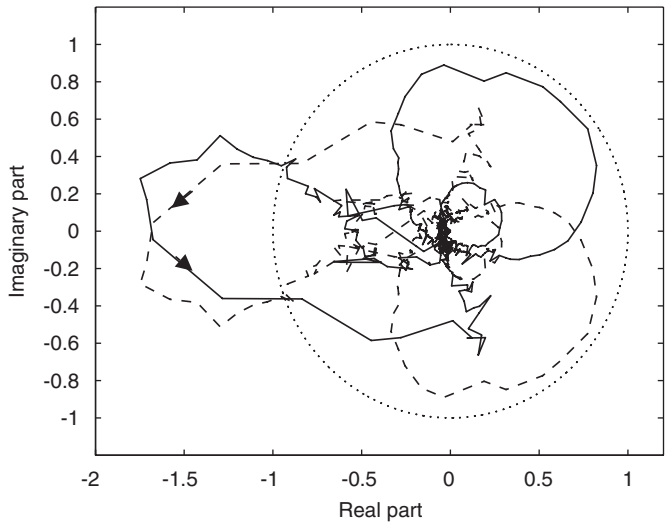

Fig. 9. The Nyquist diagram for the controlled system: —, $G(\mathrm{i}\omega)K(\mathrm{i}\omega)$ for positive ω; - - -, $G(\mathrm{i}\omega)K(\mathrm{i}\omega)$ for negative ω; …, unit circle.

anticlockwise encirclements of the -1 point shown by the controlled OLTF is equal to the number of unstable poles in the uncontrolled OLTF [38,39]. The phase increase across the first mode confirms that this is the only unstable mode, and that it has a pair of unstable poles associated with it. The Nyquist plot for $G(\mathrm{i}\omega)K(\mathrm{i}\omega)$ therefore needs to encircle the -1 point in an anticlockwise direction twice in order for the closed-loop system to be stable. The Nyquist plot for $G(\mathrm{i}\omega)$ has no encirclements of the -1 point. To achieve two encirclements, it is clear that the controller should introduce both gain and additional phase lag near the frequency of the unstable mode.

A good choice of controller structure to achieve this is that of a phase lag compensator

$$K(s) = \frac{k(s+\beta a)}{(s+a)} \quad \text{where } \beta \geqslant 1. \tag{5}$$

The maximum lag should be close to the location of the unstable mode, which from the Bode plot in Fig. 6 is at a frequency of $\omega = 1600\,\mathrm{rads}^{-1}$. The maximum lag of the phase lag compensator in Eq. (5) occurs at an approximate frequency of $a\sqrt{\beta}$, and so good choices of values for the controller are $a = 980$, $\beta = 2.67$. These values give a good compromise between maximising the phase and gain margins. The value of k is then chosen to be 3.1 to maximise the gain margin (note that the gain/phase margins must be considered in terms of both reducing and increasing the gain/phase since two encirclements of the -1 point are required).

The resulting Nyquist plot for $G(\mathrm{i}\omega)K(\mathrm{i}\omega)$ is shown in Fig. 9. It can be seen that there are indeed two anticlockwise encirclements of the -1 point and so the controlled system should be stable. The gain margin is 4.5 dB and the phase margin is 21°, thus the closed-loop system should be reasonably robust to

plant uncertainties and changes. (If needed, the stability margins could be increased by using a higher-order controller.)

2.5. Controller implementation

The above controller was implemented on the Rijke tube. The pressure spectra with control is compared to that without control in Fig. 10, and the time domain effect of switching the controller on is shown in Fig. 11. The controller eliminates the instability, resulting in a reduction of approximately 80 dB in the microphone pressure spectrum: this represents a reduction of four orders of magnitude. The controller obtains control rapidly, with oscillation amplitudes down to 10% of their unstable levels in under 10 oscillations. Although the loudspeaker voltage is initially large in order to attain control, once control has been achieved, very little actuator effort is needed to maintain it.

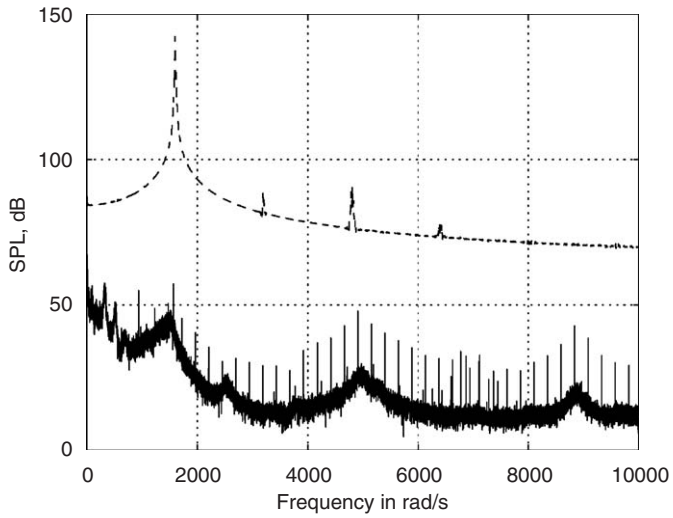

Fig. 10. The effect of control on the microphone pressure spectrum: - - -, without control; —, with control.

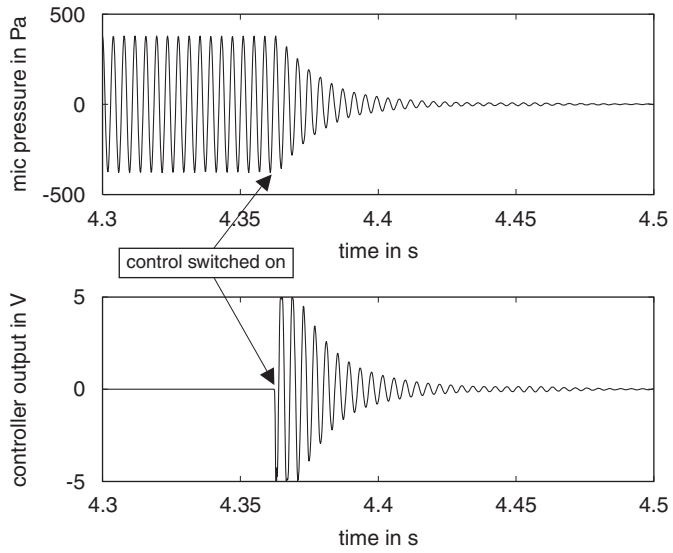

Fig. 11. The effect of control on the microphone pressure oscillations in the time domain.

2.6. Robustness study

The main benefits in using systematic controller design methods such as model-based control are seen in the controller performance at off-design conditions. In more complicated systems, for example those involving turbulent combustion or in which the flow conditions vary slightly in time, off-design conditions may occur regularly during normal operation.

In this system, in order to evaluate the off-design performance of the controller, it was necessary to introduce some disturbance to the system. This was achieved by adding a variable additional length to the top of the Rijke tube, causing the frequency of the unstable fundamental mode to vary. For a variety of different additional lengths, the controller was switched on and the time domain response of the microphone pressure oscillations recorded. The results, with the same axis scales used for all cases, are shown in Fig. 12. It is interesting to note that the unstable limit cycle amplitude increases successively with tube length, despite the microphone location being further from the pressure antinode for the fundamental mode.

The controller was able to attain control up to an increase in tube length of 19%. This compares with the empirically designed controller, which loses control for a tube length increase of less than 3%, thus

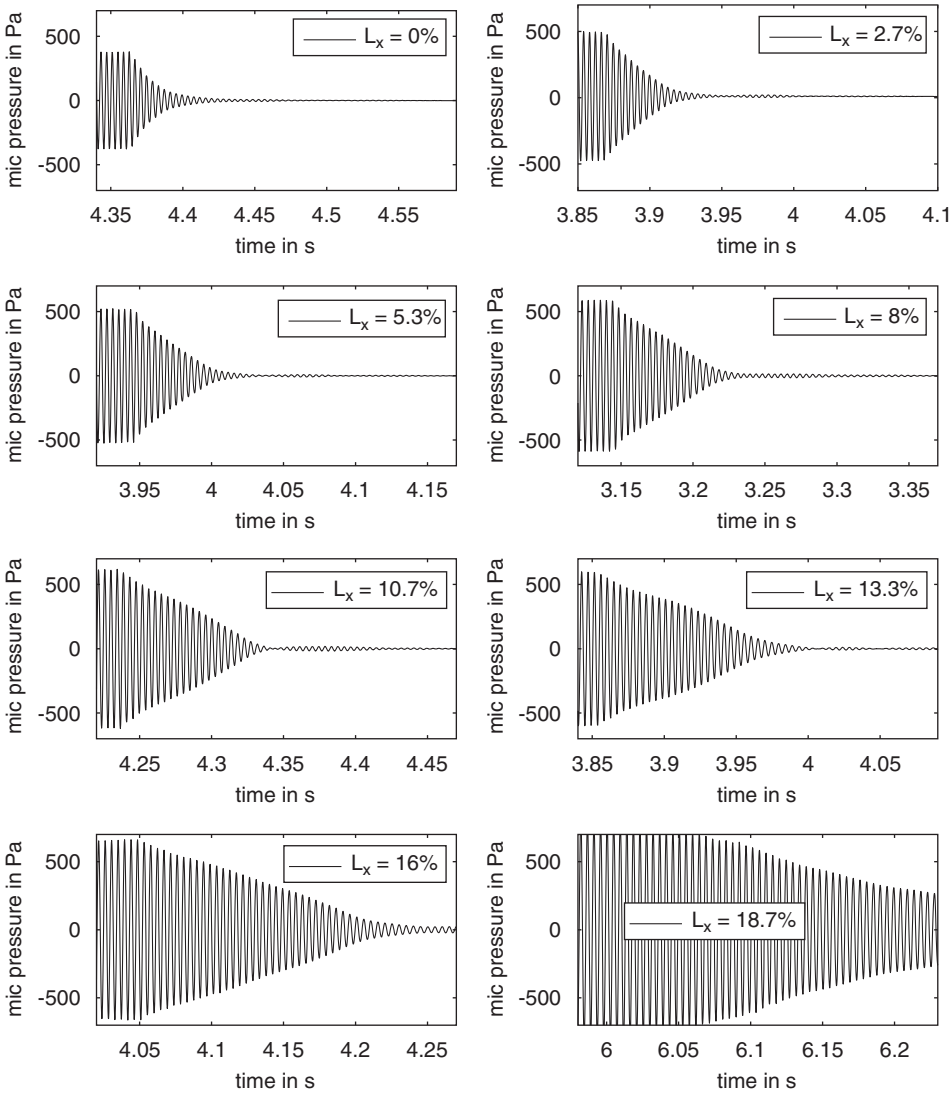

Fig. 12. The response of the microphone pressure to switching the controller on for different tube extensions.

demonstrating the robustness advantage of using systematically designed controllers. An interesting feature of the response plots is that the damping of the controlled system decreases as the tube length differs from the design length, resulting in the controller taking longer to reduce the oscillation amplitude. This corresponds to the closed-loop poles successively moving from their design point inside the left-half plane, towards the imaginary axis until they cross and enter the right-half plane, at which point the controller ceases to stabilise the system. The fact that the damping of the closed-loop system reduces at off design conditions may be important in applications where the speed of response is critical.

3. The combustion rig

The combustion rig incorporated many more of the effects limiting system measurement and controller performance in practical combustion systems, such as high noise, turbulent combustion, significant mean flow and actuation time delays. It was a blow-down atmospheric pressure rig, with the plenum and combustor comprising of cylindrical pipes, as shown in Fig. 13. A choked plate upstream of the plenum was used to ensure a steady air flow of $0.04\,\mathrm{kg\,s^{-1}}$. The plenum chamber was cylindrical along most of its length, but became annular at its downstream end. The air and fuel were premixed in a counter-rotating radial swirler which was approximately a 54% scale model of the Rolls-Royce DLE swirler. The fuel used was ethylene, supplied from a pressurised commercial cylinder. The fuel line between the cylinder and the swirler unit incorporated a pressure regulator, a plenum and a control valve. The combustion chamber was a quartz tube which was attached to the swirler unit at one end and was open and unchoked at the other.

Sensor readings were provided by Kistler piezo-electric pressure transducers mounted on side arms of the quartz tube, 640 and 730 mm from the upstream end, again using the semi-infinite line technique. Charge amplifiers were used to amplify the pressure transducer readings: a voltage of 1 V corresponded to a pressure fluctuation of 10^4 Pa. Actuation for control was obtained using a control valve on the fuel line to modulate the fuel supply. The valve was a direct drive valve (DDV) manufactured by Moog, and had a linear response to applied voltage, with 0 and 10 V corresponding to the fully closed and fully open positions, respectively. The frequency response of the valve position was measured to have a high-frequency 3 dB cutoff of approximately 370 Hz (the cut-off frequency of the fuel modulation would be slightly lower than this due to fuel-line inertia). A plenum on the fuel line upstream of the valve provided mass storage and ensured that the fuel flow rate through the valve could vary as its open area was modulated. Care was taken to minimise the length of the fuel line between the valve and the fuel injection. Control algorithms were implemented on the 32-bit DSP board, and unsteady measurements were recorded using the PC-based data-acquisition system. A more detailed description of the rig can be found in Ref. [19].

On operating the rig with an air mass flow rate of $0.04\,\mathrm{kg\,s^{-1}}$ and a fuel-line regulator pressure of 9 bar, it was found that an instability near 200 Hz occurred. This corresponded to the second harmonic in the plenum [19]. The equivalence ratio at which the instability occurred was always in the range $\phi\sim0.7$–0.9, and varied depending on the level of acoustic damping in the system. This could, for example, be varied by altering the

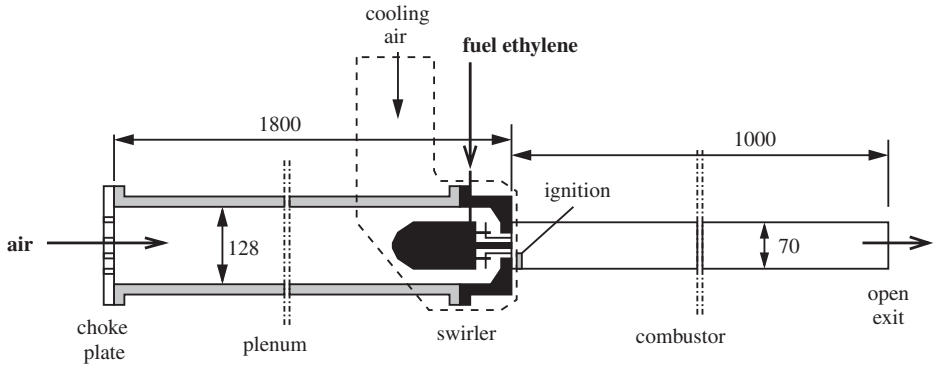

Fig. 13. A schematic of the working section of the combustion rig, dimensions in mm.

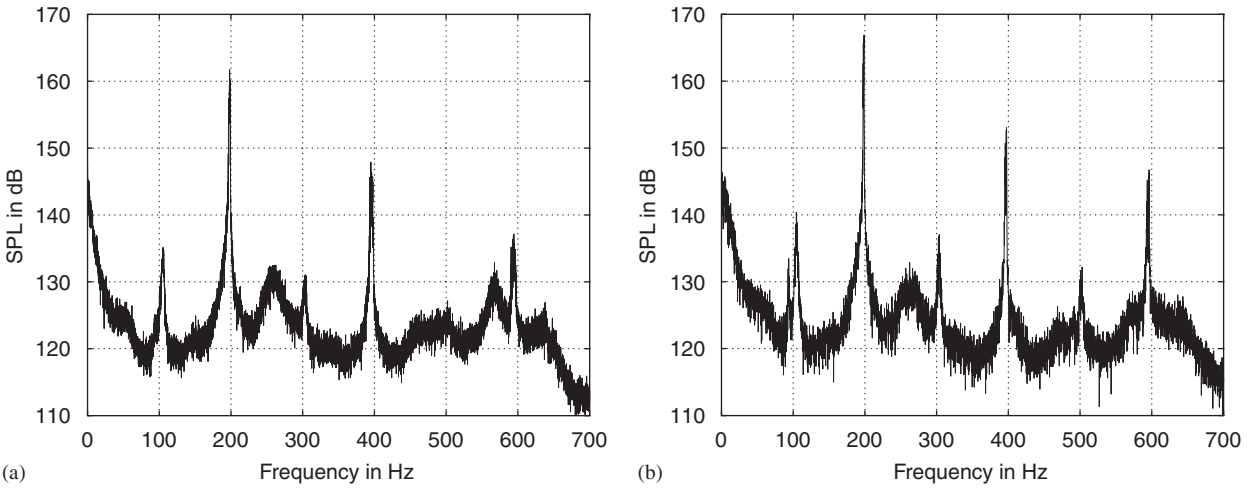

Fig. 14. The pressure spectra for the instability occurring at two different equivalence ratios: (a) $\phi\sim0.73$ and (b) $\phi\sim0.9$.

seal at the swirler/combustor interface. The lower the acoustic damping, the higher the equivalence ratio at which the instability near 200 Hz occurred and the harsher it sounded, as shown by the pressure spectra for two different equivalence ratios in Fig. 14.

The different equivalence ratios at which the instability occurred provided a framework for considering the different open-loop systems associated with the instability. The aim of this work was to design controllers which were sufficiently robust to stabilise the 200 Hz instability, no matter which equivalence ratio it occurred at.

3.1. The OLTF

The OLTF from the valve voltage, V_c, to the pressure transducer reading 64 mm from the upstream end of the quartz tube, p_{ref}, was measured using the same technique as for the Rijke tube. The valve input signal consisted of a control signal from a time delay controller which had been empirically designed previously, with a high bandwidth signal provided by a sinusoid undergoing a frequency sweep from 75 to 350 Hz. This frequency range was chosen to include the dynamics evident in the pressure spectra (Fig. 14) up to the approximate cut-off frequency of the fuel modulation. To maximise the signal available for transfer function identification across the frequency range, the amplitude of the frequency sweep was chosen to be as large as possible, subject to avoiding regular saturation of the valve. The experimental procedure involved running the rig with the valve signal first constant at 5 V, corresponding to the half open position. The equivalence ratio at which the instability near 200 Hz occurred was obtained, before switching on the valve control and frequency sweep signals.

By altering the seal at the swirler/combustor interface, the equivalence ratio at which the instability occurred was varied. The frequency responses for the instability occurring at three different equivalence ratios, $\phi\sim0.73$, $\phi\sim0.82$ and $\phi\sim0.9$, are shown in Fig. 15. All three reveal the presence of three modes in the given frequency range, one near 100 Hz, one near 200 Hz and one near 250 Hz. The mode frequencies and peak magnitudes are very similar for the three equivalence ratios, although the width of the peaks and therefore the modal damping factors vary considerably more. By considering each mode to be the result of a second-order transfer function, the phase change across the mode peaks can be used to deduce stability information. A phase increase of 180° indicates an unstable mode, while a phase decrease of 180° indicates a stable mode. The frequency responses for all three equivalence ratios confirm that the mode near 100 Hz is stable while the mode near 200 Hz is unstable. This is consistent with the very large peak near 200 Hz in the uncontrolled pressure spectra in Fig. 14. The mode near 250 Hz is harder to interpret; the amount of noise in this higher frequency region means that unwrapping the phase for the $\phi\sim0.73$ and $\phi\sim0.82$ cases can be done so as to reveal either a phase increase or decrease of 180° across the mode (see the black and grey alternatives in Fig. 15a). As no significant

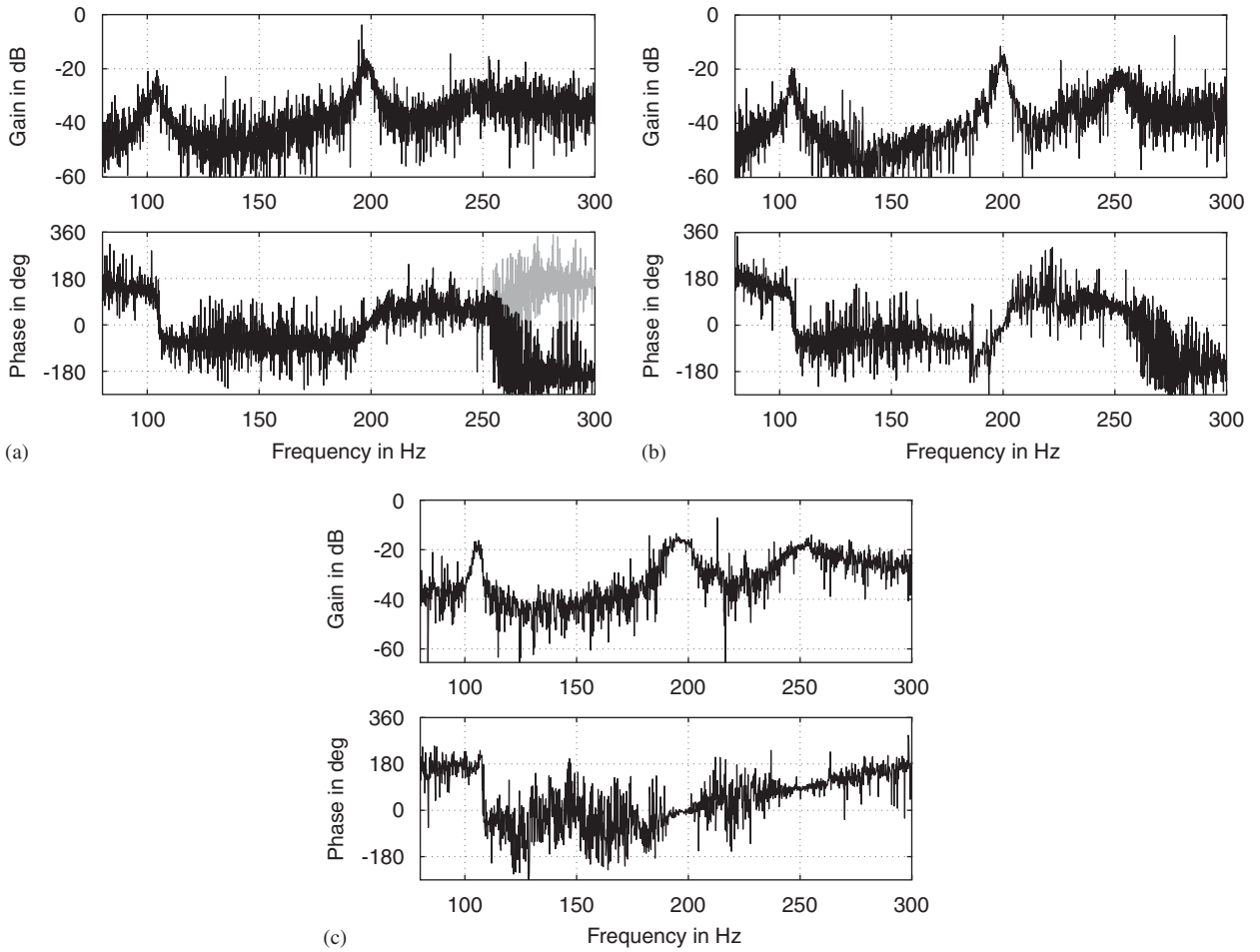

Fig. 15. Bode plots for the measured open-loop transfer function, $G(i\omega)$, at three different equivalence ratios: (a) $\phi\sim0.73$; (b) $\phi\sim0.82$; and (c) $\phi\sim0.9$. For (a): ——, phase unwrapped to give decrease near 250 Hz; —, phase unwrapped to give increase near 250 Hz.

peak near 250 Hz is seen in the pressure spectra in Fig. 14, it is clear that the mode near 250 Hz is stable and the phase should be unwrapped to give a phase decrease. Note that for $\phi\sim0.9$ the phase at high frequencies is obscured by the response to the control signal rather than the identification sine sweep signal (the phase gradient is exactly equal to the controller time delay), but the uncontrolled pressure spectrum for this case again suggests that the mode near 250 Hz is stable.

A mathematical description for $G(s)$ was based on the measured frequency response at $\phi\sim0.73$. The reason for choosing this equivalence ratio was two-fold; it was the equivalence ratio at which the most experimental data was available, and furthermore, it corresponded to the operating condition at which the instability is most commonly run. The description was obtained by hand-fitting the coefficients of a transfer function structure incorporating three second-order modal peaks. This was found to offer a better fit than formal system identification, which, due to the number of free parameters in the transfer function and the noise in the system, did not yield useful results. Furthermore, it was possible to attribute physical meanings (damping factors, resonant frequencies, etc.) to the parameters being fitted. On fitting to the measured transfer function, the fit at the frequencies of the modal peaks was deemed more important than at the frequencies between the peaks, since this would influence the controller design most strongly. The fit at the extreme frequencies of the sinusoidal frequency sweep (particularly at the upper end) was also deemed less important as the fall off in the input spectral energy here had resulted in an increased signal-to-noise ratio, and hence a large amount of uncertainty in the measured transfer function.

The structure of the transfer function used in the fitting was comprised of three second-order poles (representing the modal peaks), a second-order zero (representing the low-frequency dynamics of the fuel delivery system) to allow the phase at low frequencies to be matched, and a time delay (representing the fuel convection and wave propagation delays in the system) to allow the additional phase gradient to be captured. The result is shown in Eq. (6). The best-fit value of the damping factor for the 198 Hz mode is -0.007, corresponding to the fact that the mode is unstable with a growth rate of $8.7\,\mathrm{s}^{-1}$

$$G(s) = AG_z(s)G_{p1}(s)G_{p2}(s)G_{p3}(s)\mathrm{e}^{-T_d s},$$

where

$$\begin{aligned}
&A = 1.4\times10^{-6}, \quad T_d = 0.0012\,\mathrm{s},\\
&G_z(s) = \frac{s^2 + 2c_z\omega_z s + \omega_z^2}{\omega_z^2}, \quad \omega_z = 2\pi\times5\,\mathrm{rad}^{-1}, \quad c_z = 0.01,\\
&G_{p1}(s) = \frac{\omega_{p1}^2}{s^2 + 2c_{p1}\omega_{p1}s + \omega_{p1}^2}, \quad \omega_{p1} = 2\pi\times104\,\mathrm{rad}^{-1}, \quad c_{p1} = 0.006,\\
&G_{p2}(s) = \frac{\omega_{p2}^2}{s^2 + 2c_{p2}\omega_{p2}s + \omega_{p2}^2}, \quad \omega_{p2} = 2\pi\times198\,\mathrm{rad}^{-1}, \quad c_{p2} = -0.007,\\
&G_{p3}(s) = \frac{\omega_{p3}^2}{s^2 + 2c_{p3}\omega_{p3}s + \omega_{p3}^2}, \quad \omega_{p3} = 2\pi\times250\,\mathrm{rad}^{-1}, \quad c_{p3} = 0.012.
\end{aligned} \tag{6}$$

The frequency response of the mathematical description for $G(s)$ is compared to the measured frequency response for $\phi\sim0.73$ in Fig. 16. The aim of controller design was to design a robust controller which stabilised the instability near 200 Hz, for the range of operating conditions (i.e. equivalence ratios) at which the instability could occur. To obtain an idea of the stability/robustness margins required when basing controller design on the fitted transfer function for $\phi\sim0.73$, it is necessary to examine the difference between this fitted transfer function and each of the measured transfer functions for the three equivalence ratios in Fig. 15. For the 198 Hz peak, the maximum magnitude difference is very small; all three measured transfer functions are very similar here. The maximum magnitude difference increases slightly for the 104 Hz peak, but is largest for the 250 Hz peak where the difference between the fitted transfer function and the magnitude for $\phi\sim0.9$ is approximately 8 dB. The required gain margin therefore depends on which modes limit the system stability, but a minimum of 8 dB gives a good guide. The required phase margin is more difficult to estimate,

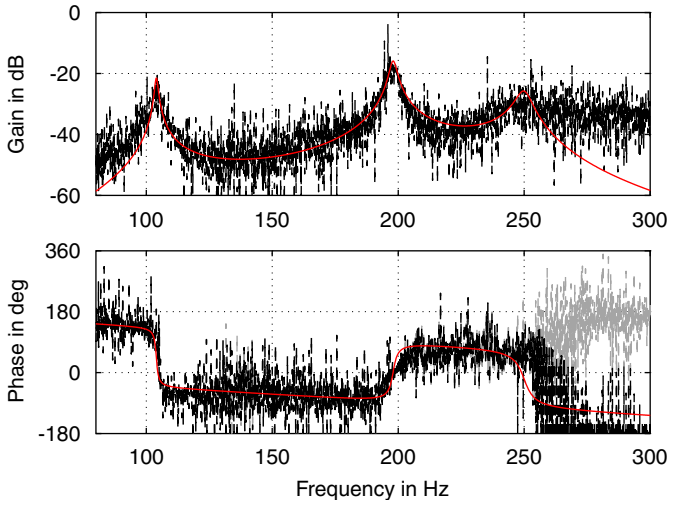

Fig. 16. Comparison of the frequency responses of $G(\mathrm{i}\omega)$ for the measured data ($\phi\sim0.73$) and mathematical approximation.

particularly as the phase information for $\phi \sim 0.9$ is almost meaningless above 200 Hz. However, it is clear that a large phase margin is advisable, ideally in excess of 45°.

3.2. Controller design

Based on the mathematical description for $G(s)$, two controllers were designed to stabilise the combustion system. It was important to ensure that the controller designs were robust to allow for inaccuracies in the description for $G(s)$, and also to ensure that stability is maintained at different equivalence ratios exhibiting the same instability, but with slightly different frequency responses. The control system is based on one sensor measurement and one actuator signal and so is single-input single-output (SISO). This enabled Nyquist techniques to be used in the design of two robust controllers.

The Nyquist plot for the mathematical description of $G(s)$ is shown in Fig. 17. The open-loop system has one unstable mode which corresponds to two unstable poles. Assuming a negative feedback control system (see Fig. 8), the Nyquist plot for $G(s)K(s)$ therefore needs to encircle the -1 point in an anticlockwise direction twice in order for the closed-loop system to be stable [38,39]. It is clear that the controller will need to provide both gain and a phase change around 200 Hz in order for the required encirclements of the -1 point to be attained.

It can also be seen from the Nyquist plot that a gain of at least 7 (= 17 dB) is required around 200 Hz in order to achieve anticlockwise encirclements of the -1 point. A larger gain may be necessary, depending on the gain-phase relationship of the controller and the degree of robustness required. The input voltage to the valve consists of a mean signal of 5 V, corresponding to the valve half-open, plus the control signal. If the magnitude of the control signal is greater than 5 V then the valve will saturate. Assuming that the pressure oscillations for a stable combustion system have amplitudes of the order of 2000 Pa, which is equivalent to a 0.2 V pressure transducer reading, a gain of greater than approximately $5/0.2 = 25$ (28 dB) will result in valve saturation. Thus for many controller structures, there will be a direct trade-off between having sufficient gain around 200 Hz to result in stability and robustness, and ensuring that the gain is small enough to avoid saturation of the valve.

3.2.1. Phase-lag compensator design

From the Nyquist Plot for $G(s)$ in Fig. 17, it is clear that a controller which introduces approximately 180° of either phase lead or phase lag around 200 Hz can be used to stabilise the system. In this first design, a controller based on a phase-lag compensator was considered. Phase-lag compensators reduce the open-loop gain at high frequencies where there is more uncertainty, and in this respect offer more potential for robust

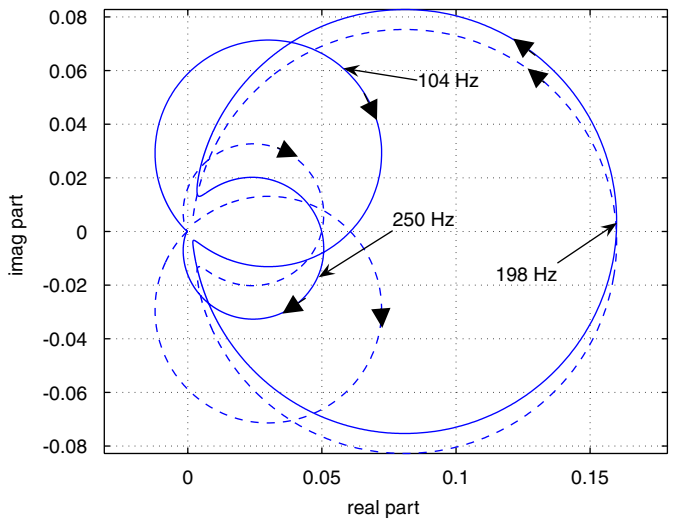

Fig. 17. Nyquist plot for the mathematical approximation of $G(i\omega)$; —, positive ω; - - -, negative ω.

design than phase-lead compensators. One drawback of phase-lag compensators with regard to this system is that they have the effect of increasing the relative gain of the low-frequency mode near 100 Hz, which tends to destabilise the system.

To obtain a sensible compromise between minimising the relative increase in the gain of the mode near 100 Hz and ensuring that enough phase lag near 200 Hz was achieved, a combination of a phase-lag compensator and an additional phase lag was used. It was necessary to raise the compensator and lag to the power of 4 in order to achieve the desired phase around 200 Hz

$$K_{\mathrm{pc}}(s) = \frac{1.1 \times 10^{14}(s+224)^4}{(s+580)^4(s+750)^4}. \tag{7}$$

The Bode plot for the controller alone is shown in Fig. 18 and the Nyquist plot for the controlled open-loop system, $G(s)K(s)$, shown in Fig. 19. The Nyquist plot confirms that the controlled OLTF exhibits two anticlockwise encirclements of the -1 point, and the closed-loop system will therefore be stable. A measure of

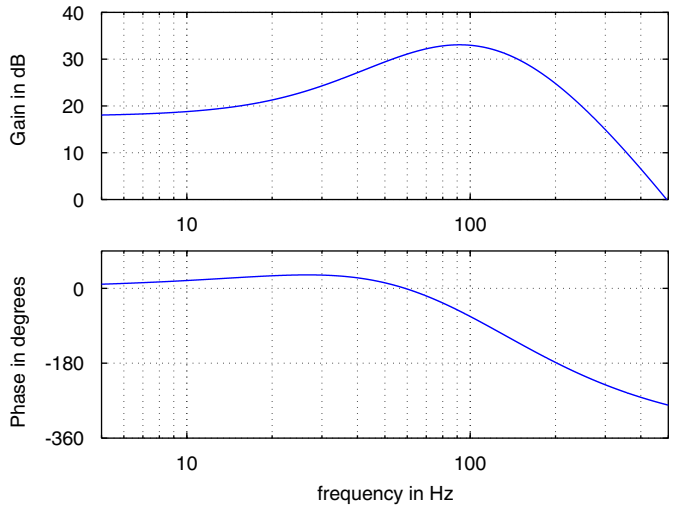

Fig. 18. Bode plot for the controller based on a phase-lag compensator, $K_{\mathrm{pc}}(\mathrm{i}\omega)$.

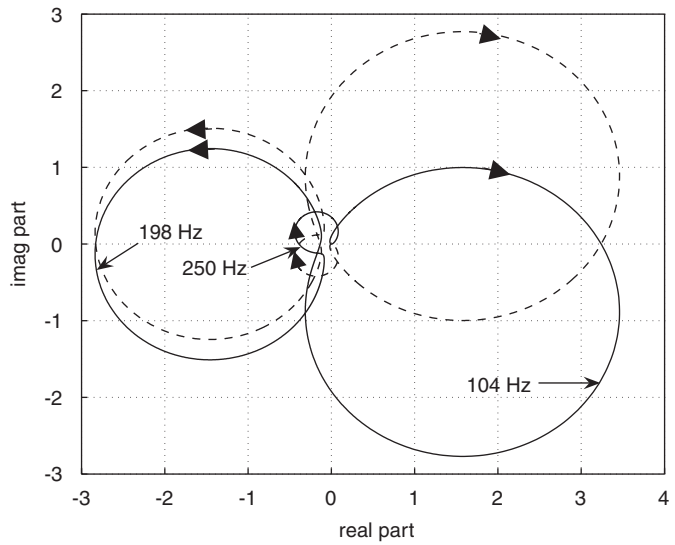

Fig. 19. Nyquist plot for $G(\mathrm{i}\omega)K_{\mathrm{pc}}(\mathrm{i}\omega)$ for the controller based on a phase-lag compensator: —, positive ω; - - -, negative ω.

the system robustness can be obtained by considering the gain and phase margins; these must be considered in terms of both reducing and increasing the gain and phase. For this controller, the gain and phase margins are approximately 9 dB and 60°, respectively. Furthermore, the gain of the controller near 200 Hz is less than 28 dB, hence valve saturation should not significantly affect the controller performance.

3.2.2. Notch filter design

A notch filter can be also be used to introduce the required phase change near 200 Hz. It has the added benefit that its gain can be chosen to be large over a relatively narrow passband, and the region of high gain and 180° phase change correspond to one another, which is advantageous for this system. A notch filter of the form

$$K_{\mathrm{nf}}(s) = \frac{1.15 \times 10^{13}}{(s^2 + 500s + 1240^2)^2} \tag{8}$$

was used. The Bode plot for the controller is shown in Fig. 20 and the Nyquist plot for the controlled open-loop system shown in Fig. 21. The gain and phase margins for the controller are approximately 14 dB and 56°, respectively. Once again, the gain of the controller near 200 Hz is less than 28 dB, hence valve saturation should not significantly affect the controller performance.

3.3. Controller implementation

The controllers were implemented experimentally on the combustion rig. This was performed at two equivalence ratios, $\phi \sim 0.73$, which represented a typical "low" equivalence ratio, and $\phi \sim 0.86$, which represented a typical "high" equivalence ratio. The performance of both controllers was compared to the "datum" time delay controller, $K_{\mathrm{td}}(s) = 10\mathrm{e}^{-0.005s}$, which had been designed empirically previously. At moderate equivalence ratios ($\phi \sim 0.75$), this controller achieved a reduction of 29 dB in the transducer pressure spectrum and did not result in regular saturation of the valve. Based on the mathematical description of the OLTF presented earlier, its gain and phase margins were 4 dB and 41°, respectively.

It should be noted that as the controllers were designed using linear theory, they would strictly only be expected to suppress the unstable growth of small (linear) disturbances, rather than to stabilise an unstable system which has already developed a nonlinear limit cycle. This corresponds with typical requirements for such controllers; the implications of instability in heavy-duty gas turbines are often so severe that suppressing the growth to instability is the more practical requirement. In this section, the controllers are activated from

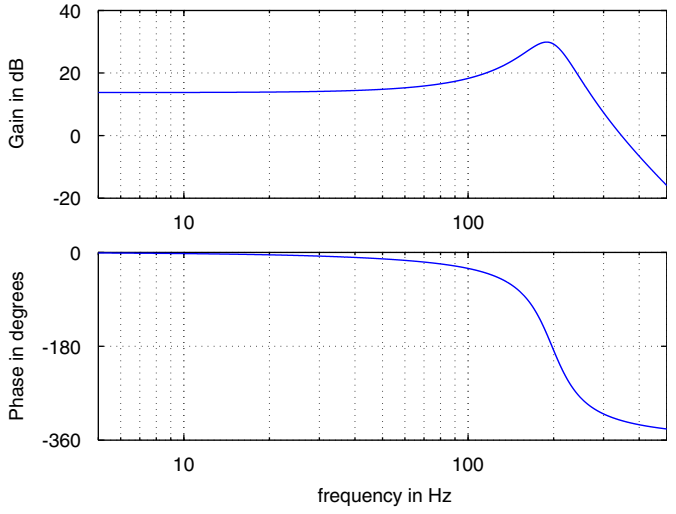

Fig. 20. Bode plot for the notch filter controller, $K_{\mathrm{nf}}(\mathrm{i}\omega)$.

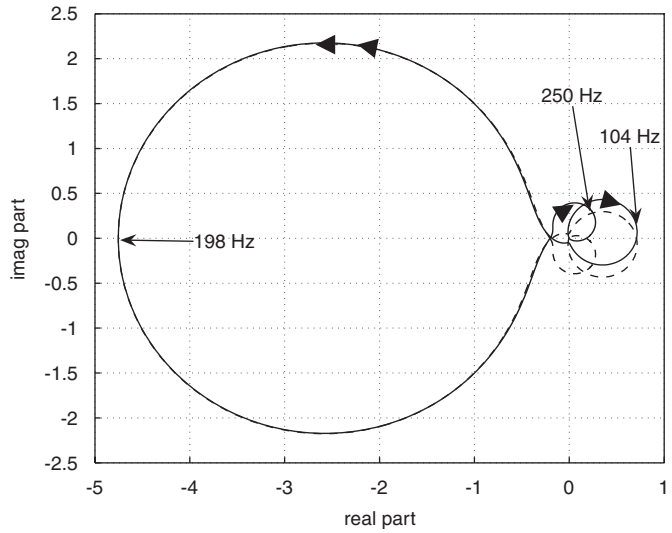

Fig. 21. Nyquist plot for $G(i\omega)K_{nf}(i\omega)$ for the notch filter controller: —, positive ω; - - -, negative ω.

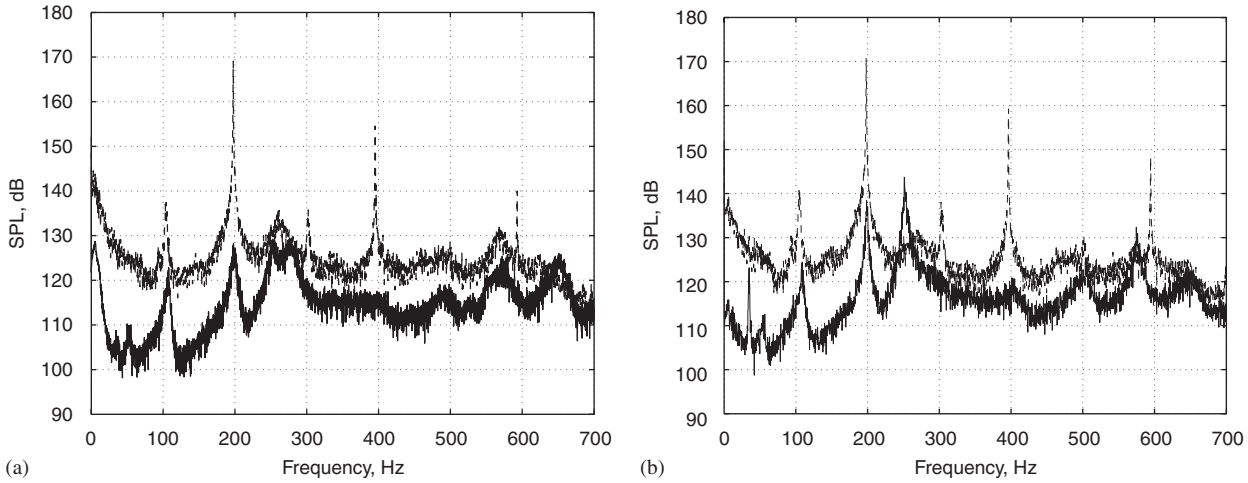

Fig. 22. Pressure spectra 64 cm from upstream end of combustor with and without control for the phase-lag compensator design. (a) $\phi\sim0.73$ and (b) $\phi\sim0.86$. —, controller on; - - -, controller off.

within an already established limit cycle, and so are being tested under more challenging conditions than they were designed for.

3.3.1. Phase-lag compensator

The effect of the phase-lag compensator controller was considered at equivalence ratios of $\phi\sim0.73$ and $\phi\sim0.86$. The resulting pressure spectra at the combustor pressure transducer are shown in Fig. 22, with the time domain effect of the controller shown in Fig. 23. For both equivalence ratios, control significantly reduces the size of the 198 Hz spectral peak and its harmonics. In the time domain, it is clear that more control authority is required to initially attain control than to maintain it once it has been achieved. For $\phi\sim0.73$ the reduction in the 198 Hz spectral peak is 41 dB, with the reduction in the maximum spectral level 40 dB. The controller acts to suppress the instability within a second of being switched on, and the valve does not saturate once control is achieved. For $\phi\sim0.86$ the reduction in the 198 Hz spectral peak is 33 dB, with the reduction in the maximum spectral level 27 dB. The controller now takes significantly longer to suppress the instability and

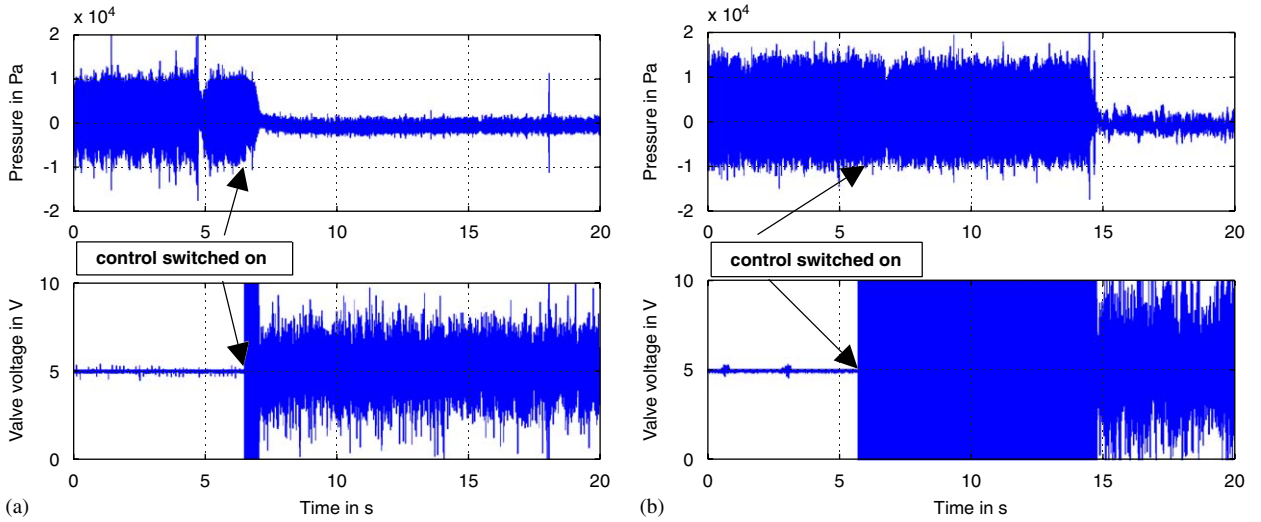

Fig. 23. Effect of the phase-lag compensator controller on the combustor pressure 64 cm from upstream end of combustor and the valve input signal: (a) $\phi\sim0.73$ and (b) $\phi\sim0.86$.

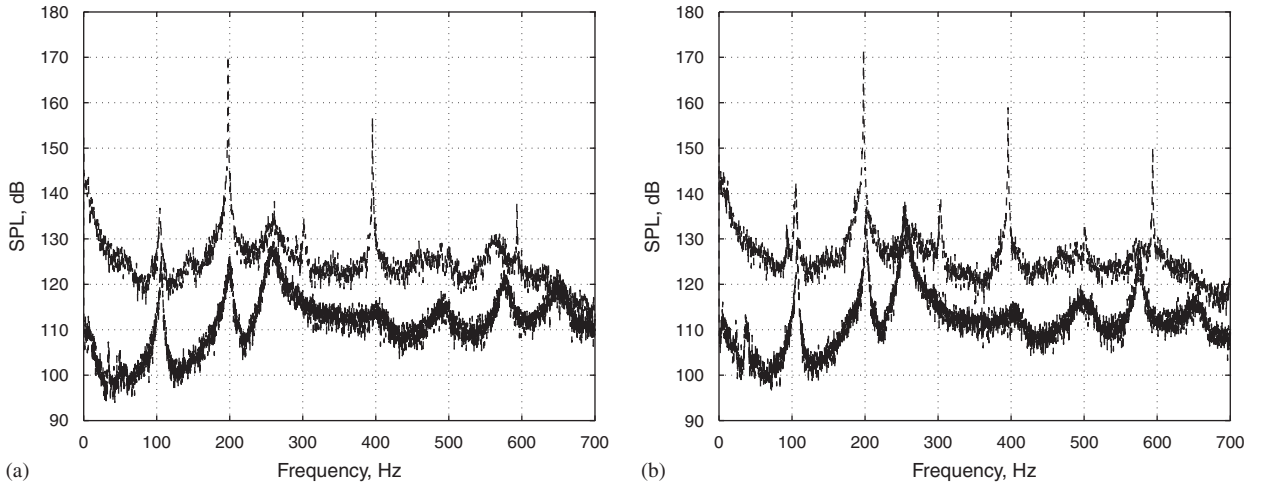

Fig. 24. Pressure spectra 64 cm from upstream end of combustor with and without control for the notch filter controller: (a) $\phi\sim0.73$; (b) $\phi\sim0.86$: —, controller on; - - -, controller off.

the valve occasionally saturates. The time taken to achieve control was 9 s, although this was not found to be repeatable. The increase in time to achieve control is most probably due to a combination of a valve saturation limiting the control authority and a change in the nonlinear limit cycle characteristics under these harsher instability conditions. The nonlinear effects which give rise to limit cycles in combustion instabilities are not well-understood [40,25], and so speculating further on the nonlinear effects such as the nonrepeatable time-to-control are beyond the scope of this paper.

3.3.2. *Notch filter*

The effect of the notch filter controller was again considered at equivalence ratios of $\phi\sim0.73$ and $\phi\sim0.86$. The pressure spectra at the pressure transducer are shown in Fig. 24, and the effect of switching control on this pressure signal and the valve input signal are shown in Fig. 25. For $\phi\sim0.73$ the reduction in the 198 Hz spectral peak is 44 dB, with the reduction in the maximum spectral level 41 dB. The controller again acts to suppress the instability within a second of being switched on, and the valve signal oscillates with an average

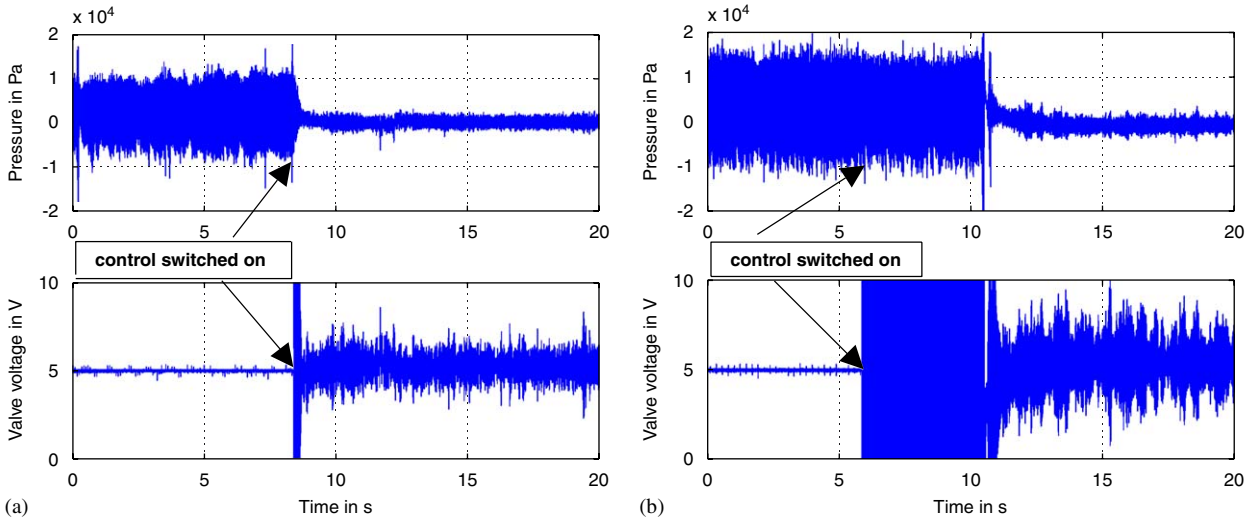

Fig. 25. Effect of the notch filter controller on the combustor pressure 64 cm from upstream end of combustor and the valve input signal: (a) $\phi\sim0.73$ and (b) $\phi\sim0.86$.

Table 1
Summary of controller performances for the atmospheric pressure combustion rig

	Controller					
	Time delay (datum)		Phase compensator		Notch filter	
Equiv. ratio	0.75	0.86	0.73	0.86	0.73	0.86
dB reduction	29	No control	40	27	41	34
Time-to-control (s)	<0.6	—	<0.6	~5 (not repeatable)	<0.3	~10 (not repeatable)

amplitude of only 1.5 V, which is well within the limits of saturation. For $\phi\sim0.86$ the reduction in the 198 Hz spectral peak is 35 dB, with the reduction in the maximum spectral level 34 dB. The controller now takes significantly longer to suppress the instability, in this case approximately 5 s, although the time to achieve stability was not repeatable. While trying to achieve stability, the valve saturates, but once control is achieved the valve signal is again well within the limits of saturation. Of the two controllers, the notch filter offers the slightly better combination of noise reduction, robustness and avoiding valve saturation.

The performance of the phase compensator, notch filter and datum time delay controllers are summarised in Table 1.

4. Conclusions

It has been shown that it is possible to accurately measure the open-loop transfer function (OLTF) of an unstable system, if a controller which stabilises the system can be found empirically. Then, using an actuator signal comprising the control signal and a high bandwidth identification signal, and measuring the effect on the sensor, the OLTF needed for model-based controller design can be measured.

The unstable OLTF of a Rijke tube with a microphone for sensing and a loudspeaker for actuation was measured experimentally using this technique. It confirmed that only the fundamental mode of the Rijke tube was unstable, which was consistent with the microphone pressure spectrum in the absence of control. A mathematical form for the OLTF, based a linear acoustic wave model and time-lag heat release model, was shown to be consistent with the measured OLTF for certain values of the heat release time delay. Based on the measured OLTF, a stabilising controller in the form of a phase-lag compensator was designed using Nyquist

techniques. On implementing this controller, the system was rapidly stabilised, reducing the microphone pressure by approximately 80 dB. A variable additional length at the top of the Rijke tube was used to perform a robustness study. The controller was able to control the instability up to an increase in tube length of 19%; this was significantly greater than for the empirically designed controller, which lost control at a tube length increase of less than 3%. This demonstrated one of the primary advantages of using systematic design techniques, such as model-based control, in controller design.

An unstable atmospheric pressure combustion rig with an instability near 200 Hz was then considered. The sensor for control was a pressure transducer mounted on the combustion chamber, with actuation provided by a fuel flow valve. To measure the OLTF from the valve input signal to the pressure transducer reading, a valve signal comprising a control signal from an empirically designed time delay controller and an identification signal in the form of a sinusoidal frequency sweep was used. For a given air mass flow rate and fuel-line regulator pressure, the equivalence ratio at which instability occurred was found to depend on the acoustic damping in the system. This enabled the OLTF to be measured for the instability occurring at three different equivalence ratios. The three transfer functions were seen to be sufficiently similar to be stabilised by the same controller, subject to the controller being designed using robust techniques. A mathematical description for the OLTF was fitted to the measured data. Using the mathematical description along with Nyquist techniques, two robust controllers were designed to stabilise the system. Both controllers had gain and phase margins greater than 9 dB and 56°, respectively. On implementing the controllers experimentally from within the large-amplitude limit-cycle resulting from the instability, both stabilised the system, eliminating the spectral peak near 200 Hz and its harmonics. The maximum spectral value was reduced by at least 39 dB at moderate equivalence ratios, which was greater than the reduction achieved by the empirically designed time-delay controller. More control authority was needed to attain control than to maintain it and the controllers did not exhibit valve saturation once control had been achieved.

Hence it has been experimentally demonstrated that it is possible to measure the OLTF of unstable combustion systems. Based on the OLTF, it is possible to design linear robust model-based controllers which stabilise the system well-beyond the operating condition which they were designed for. Furthermore, as well as preventing the exponential growth of small (linear) unstable disturbances, these controllers may be able to attain system stability from within the large-amplitude limit cycle resulting from a developed instability.

Acknowledgements

The authors would like to gratefully acknowledge the Royal Academy of Engineering and the Engineering and Physical Sciences Research Council (EPSRC) in the UK, who supported A.S. Morgans as a Research Fellow throughout this work. The work of A.J. Riley and P. Ford in operating the combustion rig is also gratefully acknowledged.

References

[1] A. Dowling, J.E. Ffowcs Williams, *Sound and Sources of Sound*, Ellis Horwood, Chichester, UK, 1983.
[2] T. Schuller, D. Durox, S. Candel, Dynamics of and noise radiated by a perturbed impinging premixed jet flame, *Combustion and Flame* 128 (2002) 88–110.
[3] G.A. Richards, M.C. Janus, Characterization of oscillations during premix gas turbine combustion, *ASME Journal of Engineering for Gas Turbines and Power* 120 (1998) 294–302.
[4] M. Zhu, A.P. Dowling, K.N.C. Bray, Self-excited oscillations in combustors with spray atomizers, *Journal of Engineering for Gas Turbines and Power—Transactions of the ASME* 123 (4) (2001) 779–786.
[5] J. Seume, N. Vortmeyer, W. Krause, J. Hermann, C. Hantschk, P. Zangl, S. Gleiss, D. Vortmeyer, A. Orthmann, Application of active combustion instability control to a heavy duty gas turbine, *Journal of Engineering for Gas Turbines and Power* 120 (1998) 721–726.
[6] H.C. Mongia, T.J. Held, G.C. Hsiao, R.P. Pandalai, Challenges and progress in controlling dynamics in gas turbine combustors, *Journal of Propulsion and Power* 19 (5) (2003) 822–829.
[7] A.A. Putnam, *Combustion Driven Oscillations in Industry*, American Elsevier, 1971.
[8] F. Culick, Combustion instabilities in liquid-fueled propulsion systems: an overview, *AGARD Conference on Combustion Instabilities in Liquid-Fueled Propulsion Systems*, 1988.

[9] G.A. Richards, D.L. Straub, E.H. Robey, Passive control of combustion dynamics in stationary gas turbines, *Journal of Propulsion and Power* 19 (5) (2003) 795–810.
[10] D.L. Gysling, G.S. Copeland, D.C. McCormick, W.M. Proscia, Combustion system damping augmentation with Helmholtz resonators, *Journal of Engineering for Gas Turbines and Power—Transactions of the ASME* 122 (2) (2000) 269–274.
[11] V. Bellucci, C.O. Paschereit, P. Flohr, F. Magni, On the use of Helmholtz resonators for damping acoustic pulsations in industrial gas turbines, no. 2001-0039, ASME, 2001.
[12] A.P. Dowling, A.S. Morgans, Feedback control of combustion oscillations, *Annual Review of Fluid Mechanics* 37 (2005) 151–182.
[13] K.R. McManus, T. Poinsot, S.M. Candel, A review of active control of combustion instabilities, *Progress in Energy and Combustion Science* 19 (1993) 1–29.
[14] A.J. Moran, D. Steele, A.P. Dowling, Active control and its applications, *Proceedings of the RTO AVT Symposium on Active Control Technology for Enhanced Performance Operational Capabilities of Military Aircraft*, *Land Vehicles and Sea Vehicles*, 2000.
[15] S. Koshigoe, T. Komatsuzaki, V. Yang, Adaptive control of combustion instability with on-line system identification, *Journal of Propulsion and Power* 15 (3) (1999) 383–389.
[16] Y. Neumeier, B.T. Zinn, Experimental demonstration of active control of combustion instabilities using real time modes observation and secondary fuel injection, *26th International Symposium on Combustion*, Naples, Italy, 1996.
[17] D. Bernier, S. Ducruix, F. Lacas, S. Candel, Transfer function measurements in a model combustor: application to adaptive instability control, *Combustion Science and Technology* 175 (2003) 993–1013.
[18] P.J. Langhorne, A.P. Dowling, N. Hooper, A practical active control system for combustion oscillations, *AIAA Journal of Propulsion and Power* 6 (1990) 324–333.
[19] A.J. Riley, S. Park, A.P. Dowling, S. Evesque, Adaptive closed-loop control on an atmospheric gaseous lean-premixed combustor, *Proceedings of the ASME Turbo Expo 2003*, no. GT-2003-38418, Atlanta, Georgia, 2003.
[20] C. Hantschk, J. Hermann, D. Vortmeyer, Active instability control with direct-drive servo valves in liquid-fueled combustion systems, *Proceedings of the Combustion Institute* 26 (1996) 2835–2841.
[21] J.M. Cohen, A. Banaszuk, Factors affecting the control of unstable combustors, *Journal of Propulsion and Power* 19 (5) (2003) 811–821.
[22] J.P. Hathout, A.M. Annaswamy, M. Fleifil, A.F. Ghoniem, A model-based active control design for thermoacoustic instability, *Combustion Science and Technology* 132 (1998) 99–138.
[23] A. Annaswamy, O.E. Rifai, M. Fleifil, J. Hathout, A. Ghoniem, A model-based self-tuning controller for thermoacoustic instability, *Combustion Science and Technology* 135 (1998) 213–240.
[24] Y.C. Chu, K. Glover, A.P. Dowling, Control of combustion oscillations via H_∞ loop-shaping, μ-analysis and integral quadratic constraints, *Automatica* 39 (2) (2003) 219–231.
[25] S.R. Stow, A.P. Dowling, Low-order modelling of thermoacoustic limit cycles, *Proceedings of the ASME TURBO EXPO—Power for Land Sea and Air*, no. GT2004-54245, Vienna, Austria, 2004.
[26] J.E. Tierno, J. C. Doyle, Multi mode active stabilization of a Rijke tube, *ASME Winter Annual Meeting: Active Control of Noise and Vibration*, Vol. DSC-Vol. 1992, p. 38.
[27] S. Murugappan, S. Acharya, D.C. Allgood, S. Park, A.M. Annaswamy, A.F. Ghoniem, Optimal control of a swirl-stabilized spray combustor using system identification approach, *Combustion Science and Technology* 175 (2003) 55–81.
[28] J.W.S. Rayleigh, *The Theory of Sound*, Vol. II, Dover, New York, 1945.
[29] S. Hoffmann, G. Weber, H. Judith, J. Hermann, A. Orthmann, Application of active combustion control to siemens heavy duty gas turbines, *Proceedings of the RTO AVT Symposium on Gas Turbine Engine Combustion, Emissions and Alternative Fuels*, Lisbon, Portugal, 1998.
[30] J.R. Hibshman, J.M. Cohen, A. Banaszuk, T.J. Anderson, H.A. Alholm, Active control of combustion instability in liquid-fueled sector combustor, *ASME-99-GT-215*, 1999.
[31] J.M. Cohen, N.M. Rey, C.A. Jacobson, T.J. Anderson, Active control of combustion instability in a liquid-fueled low-nox combustor, *Journal of Engineering for Gas Turbines and Power* 121 (2) (1999) 281–284.
[32] P.J. Dines, Active Control of Flame Noise, PhD Thesis, University of Cambridge, 1983.
[33] M. Heckl, Active control of the noise from a Rijke tube, *Journal of Sound and Vibration* 124 (1988) 117–133.
[34] W. Lang, T. Poinsot, S. Candel, Active control of combustion instability, *Combustion and Flame* 70 (3) (1987) 281–289.
[35] S. Evesque, A.P. Dowling, A.M. Annaswamy, Adaptive algorithms for control of combustion, *Proceedings of the AVT Symposium*, Braunschweig, Germany, 2000.
[36] S. Evesque, Adaptive Control of Combustion Oscillations, PhD Thesis, Cambridge University Engineering Department, 2000.
[37] A.P. Dowling, Nonlinear self-excited oscillations of a ducted flame, *Journal of Fluid Mechanics* 346 (1997) 271–290.
[38] G.F. Franklin, J.D. Powell, A. Emami-Naeini, *Feedback Control of Dynamic Systems*, fourth ed., Prentice-Hall, Englewood Cliffs, NJ, 2002.
[39] R.C. Dorf, R.H. Bishop, *Modern Control Systems*, ninth ed., Prentice-Hall, Englewood Cliffs, NJ, 2001.
[40] A.A. Peracchio, W.M. Proscia, Nonlinear heat-release/acoustic model for thermoacoustic instability in lean premixed combustors, *ASME Journal of Engineering for Gas Turbines and Power* 121 (3) (1999) 415–421.